Steering the wind using LES of yaw-driven power optimization in wind farms

Oumkalthoum M'hamdi[1], *Abdelmalek* Bouaziz[1], and *Radouan* Boukharfane[1,*]

[1]College of Computing, Mohammed VI Polytechnic University (UM6P), Benguerir, Morocco

Abstract. This study investigates wake steering in a 4×6 wind farm of 24 NREL 5 MW turbines using high-fidelity Large-Eddy Simulations (LES) coupled with the Actuator Line Method (ALM). Two control strategies are compared: a conventional *Greedy* mode where each turbine maximizes its own power, and a *Cooperative* mode optimized with the `FLORIS` framework through coordinated yaw misalignment. The cooperative strategy increases total mean power from 28.2 MW to 34.4 MW (+21.8%) while reducing front-row loads and enhancing wake recovery, leading to downstream power gains up to +80%. Temporal metrics reveal reduced periodicity and lower spectral coherence, indicating smoother and less correlated power dynamics. Overall, cooperative yaw control improves wake mixing, balances aerodynamic loading, and significantly enhances global energy capture efficiency.

1 Introduction

The increasing global demand for renewable and sustainable energy sources has positioned wind power as a leading contributor to the ongoing energy transition. Modern wind farms typically comprise large arrays of wind turbines installed within spatially constrained areas. The aerodynamic wakes generated by upstream turbines interact significantly with the inflow of downstream turbines, degrading overall farm efficiency and causing power generation reductions of 10–25% in large-scale onshore and offshore configurations [1]. A comprehensive understanding and mitigation of wake effects therefore constitute a central challenge in modern wind farm design and operation.

Among various control strategies developed to reduce wake-induced power losses, yaw control has emerged as one of the most effective approaches. By intentionally yawing a rotor relative to the incoming wind direction, the resulting wake can be deflected laterally, allowing more undisturbed flow to reach downstream turbines. This mechanism, commonly referred to as *wake steering*, has been shown to improve aggregate farm-level power output. However, determining the optimal yaw configuration represents a complex multi-objective optimization problem, requiring careful trade-offs between upstream power losses and overall farm-wide gains.

In conventional "greedy" operating mode, each turbine aligns its rotor perpendicular to the wind to maximize individual power extraction, without considering wake impacts on neighboring turbines. Conversely, "cooperative" or "coordinated" yaw control strategies aim to optimize the collective power production of the entire farm by adjusting all turbine yaw

*e-mail: radouan.boukharfane@um6p.ma

angles simultaneously. Developing and validating such strategies requires high-fidelity modeling frameworks capable of accurately reproducing intricate wake dynamics under yawed inflow conditions [2].

In the present work, we investigate wake steering performance in a wind farm consisting of 24 NREL 5-MW turbines arranged in a 4×6 layout. The simulations combine the *Actuator Line Method* (ALM) with *Large-Eddy Simulation* (LES) to resolve unsteady, three-dimensional wake structures across the array. Yaw angles are optimized using the *FLORIS* framework [3], which employs reduced-order, physics-based wake models to determine configurations maximizing total farm power. Two operating scenarios are compared: (i) a reference case where all turbines align with the incoming wind, and (ii) an optimized configuration where each turbine adopts FLORIS-predicted yaw angles. Through comparative analysis of wake dynamics, recovery characteristics, and total power output, we quantify the benefits of yaw steering and elucidate the flow mechanisms underlying cooperative control in large-scale wind farms.

2 Numerical Setup

2.1 Governing Equations

The fluid motion is governed by the incompressible Navier–Stokes equations, supplemented by a subgrid-scale (SGS) model to represent unresolved turbulent motions. Within the LES framework, a spatial filtering operator, denoted by $\widetilde{(\cdot)}$, decomposes the flow field into resolved and subgrid components. The governing equations for the filtered velocity field $\widetilde{\boldsymbol{u}} = (\widetilde{u}_x, \widetilde{u}_y, \widetilde{u}_z)$ are:

$$\nabla \cdot \widetilde{\boldsymbol{u}} = 0, \tag{1}$$

$$\frac{\partial \widetilde{\boldsymbol{u}}}{\partial t} + \widetilde{\boldsymbol{u}} \cdot \nabla \widetilde{\boldsymbol{u}} = -\frac{1}{\rho} \nabla \widetilde{p} + \nu \nabla^2 \widetilde{\boldsymbol{u}} + \nabla \cdot \widetilde{\boldsymbol{\tau}}^{\mathrm{sgs}} + \boldsymbol{f}, \tag{2}$$

where ρ and ν denote fluid density and kinematic viscosity, $\widetilde{p}$ is the filtered pressure, and $\boldsymbol{f}$ represents the external body force. The subgrid-scale stress tensor, $\widetilde{\tau}_{ij}^{\mathrm{sgs}} = \widetilde{u_i u_j} - \widetilde{u}_i \widetilde{u}_j$, accounts for momentum transfer between resolved and unresolved scales.

The subgrid stresses are modeled using the classical Boussinesq hypothesis [4], which assumes an analogy between turbulent and viscous stresses through turbulent viscosity ν_t:

$$\widetilde{\tau}_{ij}^{\mathrm{sgs}} = \nu_t \left(\frac{\partial \widetilde{u}_i}{\partial x_j} - \frac{\partial \widetilde{u}_j}{\partial x_i} \right) - \frac{2}{3} \nu_t \frac{\partial \widetilde{u}_k}{\partial x_k} \delta_{ij}. \tag{3}$$

The eddy viscosity ν_t is dynamically evaluated according to the Germano–Lilly procedure: $\nu_t = (C_s^d \Delta)^2 \sqrt{2 \widetilde{\mathcal{S}}_{ij} \widetilde{\mathcal{S}}_{ij}}$, where $\widetilde{\mathcal{S}}_{ij}$ is the resolved strain-rate tensor, Δ represents the characteristic LES filter width, and C_s^d is the dynamically computed Smagorinsky coefficient.

In the actuator line framework, the body force term $\boldsymbol{f}$ in Eq. (2) represents the action of wind turbines on the surrounding flow field [5]. This force distribution is applied along rotating lines corresponding to turbine blades, capturing aerodynamic loading without explicitly resolving blade geometry or employing moving meshes.

2.2 Actuator Line Model

In the ALM, each turbine blade is represented by a continuous distribution of body forces applied along its quarter-chord line, rather than being explicitly resolved in the computational

mesh. The flow is solved in a global Cartesian coordinate system (x, y, z) corresponding to streamwise, cross-stream, and vertical directions. The azimuthal position of a blade is defined by angle θ, with successive blades separated by $\Delta\theta = 2\pi/b$, where b denotes the number of blades ($b = 3$ for the NREL 5 MW turbine). A local rotating coordinate system (r, θ, x) attached to each blade evaluates the relative velocity between incoming flow and the blade element [6].

At each actuator point, instantaneous aerodynamic forces are computed dynamically using tabulated airfoil data for lift and drag coefficients. Denoting (u_x, u_y, u_z) as interpolated velocity components at actuator points, Ω as rotor angular velocity, and r as local radius, the relative azimuthal velocity is:

$$u_\theta = \Omega r - u_y \cos\theta + u_z \sin\theta.$$

The inflow and attack angles are defined as $\phi = \arctan(u_x/u_\theta)$ and $\alpha = \phi - \gamma$, where γ represents local blade twist and pitch. The lift and drag forces per unit span are:

$$f_L = u_{\text{rel}}^2 c C_L/2, \quad f_D = u_{\text{rel}}^2 c C_D/2,$$

where $u_{\text{rel}} = \sqrt{u_\theta^2 + u_x^2}$ is the local relative velocity, c is the local chord length, and C_L, C_D are lift and drag coefficients including three-dimensional corrections. These sectional forces are projected from the blade frame to the global coordinate system as:

$$f_x = -(f_L \cos\phi + f_D \sin\phi), \tag{4}$$
$$f_y = -(f_L \sin\phi - f_D \cos\phi)\cos\theta, \tag{5}$$
$$f_z = (f_L \sin\phi - f_D \cos\phi)\sin\theta. \tag{6}$$

To prevent numerical oscillations and ensure smooth force distribution, body forces are projected onto the Eulerian grid using a regularized kernel function. A commonly adopted approach employs a Gaussian smoothing kernel [7]:

$$\eta_\epsilon = \frac{1}{\epsilon^3 \pi^{3/2}} \exp\left(-\frac{d^2}{\epsilon^2}\right), \tag{7}$$

where $d = \sqrt{(x_{i,j,k} - x^a)^2 + (y_{i,j,k} - y^a)^2 + (z_{i,j,k} - z^a)^2}$ is the distance between grid point (i, j, k) and actuator point (x^a, y^a, z^a), and ϵ denotes the kernel width. Following recommendations from Martínez-Tossas et al. [8], a constant value of $\epsilon = 2.5\Delta_{\text{grid}}$ is used throughout this work.

Because the Gaussian kernel decays slowly, its effective support must be truncated and renormalized, which becomes computationally expensive. To address this limitation, a compact kernel function is adopted:

$$\eta_\epsilon = \frac{a}{4\pi\epsilon^3} \frac{4 - (d/\epsilon)^2}{1 + (d/\epsilon)^2} H(2 - d/\epsilon), \quad a = \frac{3}{22 - 15\arctan 2}, \tag{8}$$

where H is the Heaviside function. This compact formulation provides finite support of 2ϵ, ensuring force conservation while improving computational efficiency.

3 Computational Setup

The simulated wind farm consists of an aligned 4×6 array of turbines with streamwise and spanwise spacings of $5D$ and $4D$, respectively, where D denotes rotor diameter. This

configuration is representative of typical offshore wind farm layouts and provides a relevant framework for investigating wake interactions and control strategies. Two farm-level yaw configurations are analyzed under below-rated inflow conditions corresponding to uniform free-stream velocity $U_\infty = 8\ \mathrm{m\,s^{-1}}$ and turbulence intensity $I = 6\%$.

The first configuration, hereafter referred to as the *Greedy* case, corresponds to baseline operation where all turbines align with the incoming wind to maximize individual power extraction. No coordination among turbines is considered, and wake interactions are neglected in the control strategy. The second configuration, the *Cooperative* case, represents an optimized yaw setup where each turbine is intentionally misaligned to deflect its wake away from downstream machines, thereby enhancing overall array power output.

Optimal yaw angles for the cooperative scenario are determined using the *FLORIS* framework following the methodology of Gebraad et al. [9]. The optimization relies on a calibrated analytical wake model based on the standard Jensen model combined with wake redirection submodels. FLORIS calibration uses two-turbine reference data to ensure accurate wake deflection and power predictions. The optimization employs a Sequential Least Squares Programming (SLSQP) algorithm to maximize total farm power output, subject to yaw angle constraints ($-30^\circ \le \gamma \le 30^\circ$) and convergence tolerance $\varepsilon_{\mathrm{tol}} = 10^{-5}$. Under these conditions, FLORIS estimates a 21.4% increase in power production for the optimized yaw configuration. The corresponding yaw angles, identical across each turbine column, are summarized in Table 1.

Table 1. Yaw angle settings (in degrees) for each turbine under *Cooperative* operational mode.

Turbine	Row #1	Row #2	Row #3	Row #4	Row #5	Row #6
T1	25.00	25.00	17.19	12.50	6.25	0.00
T2	25.00	25.00	17.19	10.94	6.25	0.00
T3	25.00	25.00	17.19	10.94	6.25	0.00
T4	25.00	25.00	17.19	10.94	6.25	0.00

Both *Greedy* and *Cooperative* configurations are subsequently simulated using the high-fidelity solver to validate FLORIS optimization results and analyze underlying wake dynamics. The computational domain extends over $35D \times 4D \times 20D$ in streamwise, spanwise, and vertical directions. The domain is discretized using a uniform grid with $\Delta x = \Delta y = \Delta z = 2.24$ m, corresponding to $1969 \times 223 \times 1127$ grid nodes (more than half a billion degrees of freedom). A uniform velocity profile is prescribed at the inlet, and flow statistics are collected over a physical averaging time of 700 s.

4 Results and Discussion

4.1 Wake Structure and Flow Visualization

The instantaneous iso-surfaces of the Q-criterion colored by spanwise velocity component ($\widetilde{u}_y$) for both configurations are shown in Fig. 1. In the *Greedy* case, wakes remain nearly aligned with the streamwise direction, displaying strong coherent vortex cores and significant wake overlap between successive rows, which reduces momentum recovery. In contrast, the *Cooperative* configuration exhibits clear lateral deflection of the wakes, indicated by alternating blue and yellow regions of $\widetilde{u}_y$, reflecting wake steering induced by yaw misalignment. This lateral displacement promotes enhanced flow mixing and faster wake recovery, thereby reducing wake interference and improving downstream velocity replenishment.

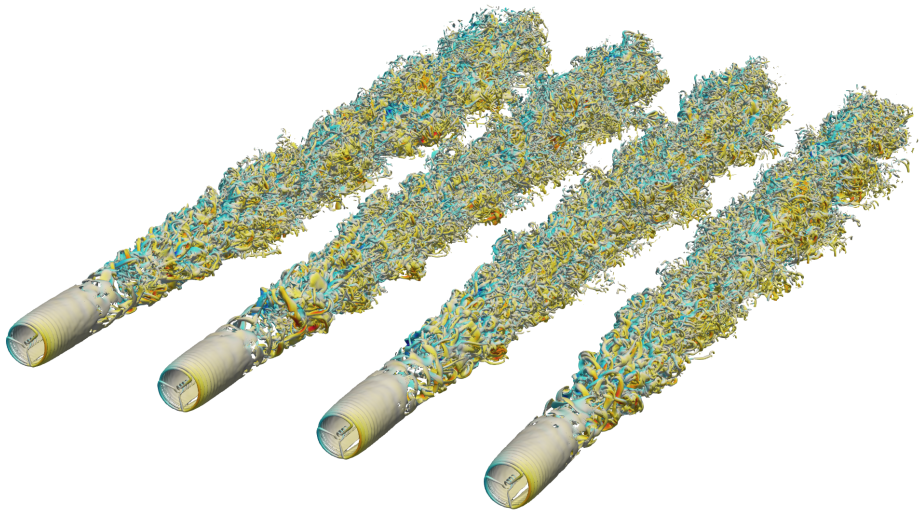

(a) *Greedy* configuration

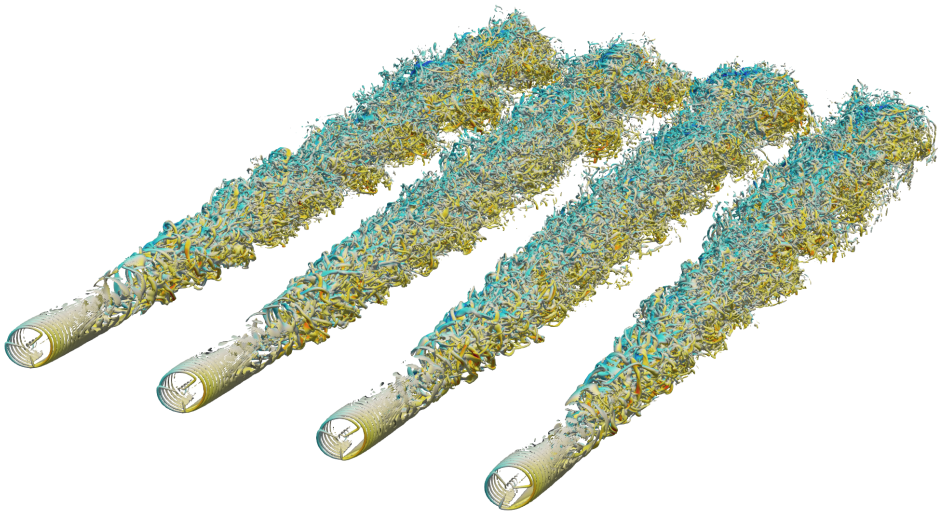

(b) *Cooperative* configuration

Figure 1. Instantaneous Q-criterion colored by spanwise velocity component for the 4×6 turbine array.

4.2 Power and Thrust Distribution

The row-wise normalized time-averaged power and thrust for the 4×6 turbine array under *Greedy* and *Cooperative* operating strategies are shown in Fig. 2. The cooperative control leads to clear overall performance enhancement, with total mean power increasing from 28.23 MW to 34.37 MW, corresponding to a +21.8% gain relative to the greedy case. The first-row turbines purposely operate below nominal output (−18% power and −13% thrust), mitigating wake intensity and redirecting higher-momentum flow toward downstream rows. Consequently, following rows experience substantial power recovery—up to +80% for the second row—and moderate thrust increases ($\approx$ +20–30%) consistent with stronger inflow

velocities. This cooperative yaw coordination achieves a more uniform load distribution and significant improvement in global energy capture compared with conventional greedy operation.

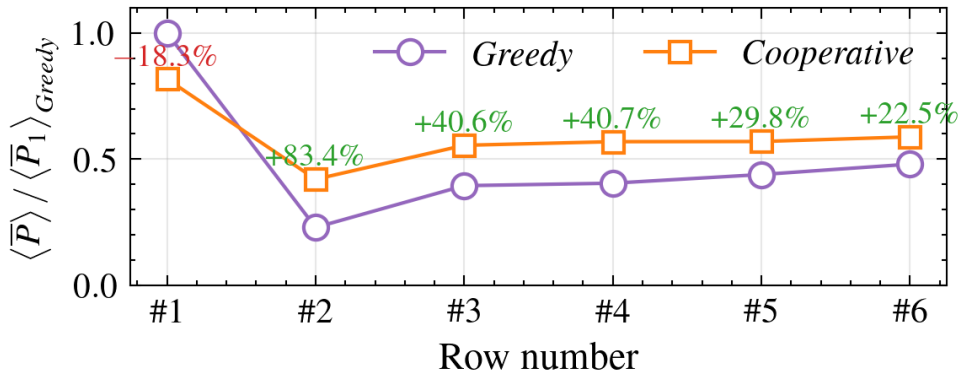

(a) Normalized time-averaged power

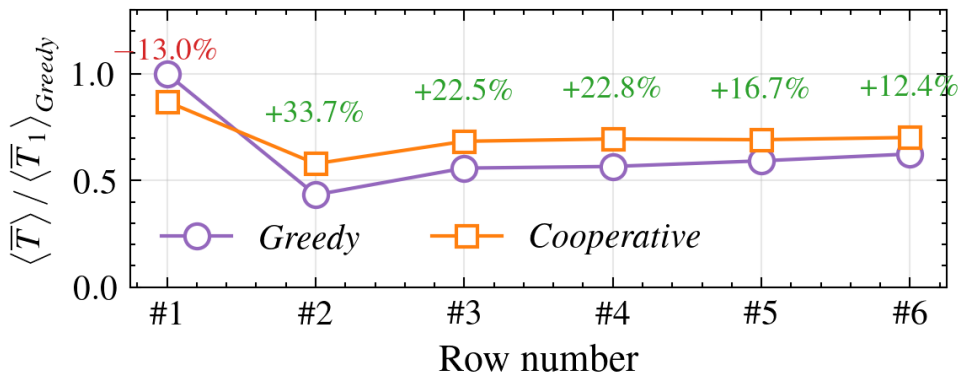

(b) Normalized time-averaged thrust

Figure 2. Time-averaged power and thrust distributions across the 4×6 wind-turbine array, normalized by corresponding mean values of first-row turbines in the greedy case.

4.3 Temporal Dynamics and Spectral Analysis

To quantify temporal dynamics and periodicity of power signals $P(t)$ produced by each turbine row, several complementary indicators are extracted from time and frequency domains. The signal is sampled with uniform timestep Δt, defining sampling frequency $f_s = 1/\Delta t$ and Nyquist frequency $f_N = f_s/2$. For each time series of length n, mean power $\overline{P}$ and fluctuation $P'(t) = P(t) - \overline{P}$ serve as the basis for statistical analysis.

The temporal correlation structure is analyzed through the normalized autocorrelation function:

$$R_{PP}(\tau) = \frac{\langle P'(t)\, P'(t+\tau) \rangle}{\langle P'(t)^2 \rangle}, \tag{9}$$

where τ denotes time lag. The first local maximum of $R_{PP}(\tau)$ beyond $\tau = 0$ defines the characteristic correlation period T_{ACF}, representing the typical recurrence time of oscillations.

The amplitude of this peak, denoted $\mathrm{ACF}_{\mathrm{peak}} = R_{PP}(T_{\mathrm{ACF}})$, quantifies periodicity strength: $\mathrm{ACF}_{\mathrm{peak}} \approx 1$ indicates strongly coherent oscillation, while values near zero indicate stochastic or broadband dynamics.

The frequency content is analyzed using the discrete Fourier transform:

$$\widehat{P}(f) = \int_{-\infty}^{\infty} P'(t)\, e^{-2\pi i f t}\, dt, \tag{10}$$

from which the one-sided power spectral density is obtained as $E(f) = |\widehat{P}(f)|^2$. The dominant frequency $f_{\max}$ maximizes $E(f)$, and the spectral period $T_{\mathrm{FFT}} = 1/f_{\max}$ is interpreted as the signal's spectral period. When $T_{\mathrm{FFT}} \approx T_{\mathrm{ACF}}$, time- and frequency-domain analyses are consistent, confirming well-defined oscillatory behavior.

The sharpness of the spectral peak is quantified through spectral signal-to-noise ratio:

$$\mathrm{SNR}_{\mathrm{spec}} = \frac{\max_f E(f)}{\langle E(f) \rangle_f}, \tag{11}$$

which measures how dominant the main frequency component is compared to the broadband background. Large $\mathrm{SNR}_{\mathrm{spec}}$ values indicate quasi-monochromatic signals, while low values correspond to turbulent or irregular fluctuations.

Finally, overall spectral complexity is characterized using normalized spectral entropy:

$$H_{\mathrm{spec}} = -\frac{1}{\log N_f} \sum_{i=1}^{N_f} p_i \log p_i, \quad p_i = \frac{E(f_i)}{\sum_j E(f_j)}, \tag{12}$$

where p_i is the normalized spectral probability density. Low H_{spec} values (close to zero) correspond to narrowband, nearly periodic signals, while $H_{\mathrm{spec}} \to 1$ indicates broadband, noisy dynamics typical of chaotic or turbulent regimes.

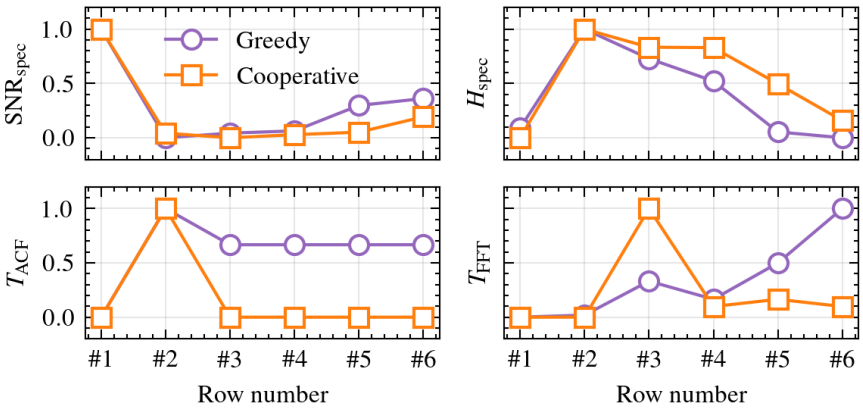

Figure 3. Temporal metrics of power fluctuations for the 4×6 turbine array under *Greedy* and *Cooperative* operation.

The four temporal indicators of power fluctuations across turbine rows for both strategies are displayed in Fig. 3. The *Cooperative* case exhibits systematically lower values of T_{ACF} and T_{FFT}, indicating reduced periodicity and shorter correlation times consistent with more stabilized, less coherent wake fields. The spectral entropy H_{spec} is slightly higher in the

Cooperative case, reflecting enhanced broadband turbulence and more uniform energy distribution across frequencies. Conversely, spectral signal-to-noise ratio SNR_{spec} is markedly lower for most rows, confirming attenuation of dominant oscillatory components. Overall, cooperative yaw coordination yields smoother, less correlated power dynamics, evidencing improved wake mixing and downstream flow recovery.

5 Conclusion

This study employed high-fidelity Large-Eddy Simulations (LES) coupled with the Actuator Line Method (ALM) to evaluate yaw-based cooperative control in a 4×6 array of NREL 5 MW turbines. Two operational strategies were compared: a conventional *Greedy* mode and an optimized *Cooperative* mode determined using the `FLORIS` framework. The cooperative strategy yielded a substantial increase in total mean power from 28.2 MW to 34.4 MW (+21.8%) while redistributing aerodynamic loads across the farm. Upstream turbines operated at reduced power and thrust, intentionally redirecting wakes and enabling enhanced downstream flow recovery, leading to power gains up to +80% in the second row.

Temporal analyses confirmed that cooperative yawing reduces periodicity and correlation in power fluctuations, indicating improved wake mixing and greater flow stability. Spectral characterization demonstrated that the cooperative mode produces broadband power dynamics with significantly attenuated dominant oscillatory components, confirming the benefits of coordinated control.

Overall, coordinated yaw control was shown to enhance both energy capture and load balance, demonstrating its effectiveness for large-scale wind farm optimization. Future work will extend this analysis to include unsteady inflow conditions, structural load assessments, and real-time control implementations for field-scale validation.

References

[1] R.J. Barthelmie, S.C. Pryor, S.T. Frandsen, K.S. Hansen, J.G. Schepers, K. Rados, W. Schlez, A. Neubert, L.E. Jensen, S. Neckelmann, Quantifying the impact of wind turbine wakes on power output at offshore wind farms, Journal of Atmospheric and Oceanic Technology **27**, 1302 (2010).

[2] T. Burton, N. Jenkins, D. Sharpe, E. Bossanyi, Wind Energy Handbook (John Wiley & Sons, 2011)

[3] National Renewable Energy Laboratory (NREL), FLORIS: Wind Farm Flow Model (2019), version 1.0.0

[4] J. Boussinesq, Essai sur la théorie des eaux courantes (Imprimerie nationale, 1877)

[5] J.N. Sørensen, W.Z. Shen, Numerical modeling of wind turbine wakes, J. Fluids Eng. **124**, 393 (2002).

[6] R. Boukharfane, Development and Validation of a Highly Scalable Finite-Volume Unstructured LES Solver for Wind Farm Flows, in *APS Division of Fluid Dynamics Meeting Abstracts* (2024), pp. L16–004

[7] P. Sørensen, A.D. Hansen, P.A.C. Rosas, Wind models for simulation of power fluctuations from wind farms, Journal of Wind Engineering and Industrial Aerodynamics **90**, 1381 (2002).

[8] L.A. Martínez-Tossas, M.J. Churchfield, S. Leonardi, Large eddy simulations of the flow past wind turbines: actuator line and disk modeling, Wind Energy **18**, 1047 (2015).

[9] P.M.O. Gebraad, F.W. Teeuwisse, J.W. Van Wingerden, P.A. Fleming, S.D. Ruben, J.R. Marden, L.Y. Pao, Wind plant power optimization through yaw control using a parametric model for wake effects—a CFD simulation study, Wind Energy **19**, 95 (2016).